Gemcitabine lipid prodrug nanoparticles: switching the lipid moiety and changing the fate in the bloodstream

Eleonore Coppens, Didier Desmaële, Timothée Naret, Sébastien Garcia-Argote, Sophie Feuillastre, Grégory Pieters, Catherine Cailleau, Jean-Louis Paul, Bastien Prost, Audrey Solgadi, et al.

Gemcitabine lipid prodrug nanoparticles: switching the lipid moiety and changing the fate in the bloodstream

Eleonore Coppens[a], Didier Desmaële[a], Timothée Naret[b], Sébastien Garcia-Argote[b], Sophie Feuillastre[b], Grégory Pieters[b], Catherine Cailleau[a], Jean-Louis Paul[c,d], Bastien Prost[e], Audrey Solgadi[e], Jean-Philippe Michel[a], Magali Noiray[a], Patrick Couvreur[a], Simona Mura[a,*]

[a]Institut Galien Paris-Saclay, UMR 8612, CNRS, Université Paris-Saclay, Faculté de Pharmacie, 5 rue Jean-Baptiste Clément, F-92296 Châtenay-Malabry cedex, France

[b]Université Paris-Saclay, CEA, INRAE, Département Médicaments et Technologies pour la Santé (DMTS), SCBM, Bat 547, 91191 Gif-sur-Yvette (France)

[c]AP-HP, Hôpital Européen Georges Pompidou, Service de Biochimie, 75015 Paris, France

[d]Lip(Sys)[2], Athérosclérose: homéostasie et trafic du cholestérol des macrophages, Université Paris-Saclay, Faculté de Pharmacie, 5 rue Jean-Baptiste Clément, F-92296 Châtenay-Malabry cedex, France

[e]SAMM, UMS IPSIT, Université Paris-Saclay, Faculté de Pharmacie, 5 rue Jean-Baptiste Clément, F-92296 Châtenay-Malabry cedex, France

[*]Corresponding author at: Institut Galien Paris-Saclay, UMR 8612, CNRS, Université Paris-Saclay, Faculté de Pharmacie, 5 rue Jean-Baptiste Clément, F-92296 Châtenay-Malabry cedex, France

E-mail address: simona.mura@universite-paris-saclay.fr *(S. Mura)*

Abstract

A simple approach to achieve a lipoprotein (LP)-mediated drug delivery is to trigger the spontaneous drug insertion into endogenous lipoproteins in the bloodstream, by means of its chemical modification. Nanoparticles (NPs) made of the squalene-gemcitabine (SQGem) conjugate were found to have a high affinity for plasma lipoproteins while free gemcitabine did not, suggesting a key role of the lipid moiety in this event. Whether the drug conjugation to cholesterol, one of the major lipoprotein-transported lipids, could also promote an analogous interaction was a matter of question. NPs made of the cholesterol-gemcitabine conjugate (CholGem) have been herein thoroughly investigated for their blood distribution profile both *in vitro* and *in vivo*. Unexpectedly, contrarily to SQGem, no trace of the CholGem prodrug could be found in the lipoprotein fractions, nor was it interacting with albumin. The investigation of isolated NPs and NPs/LPs physical mixtures provided a further insight into the lack of interaction of CholGem NPs with LPs. Although essential for allowing the self-assembly of the prodrug into nanoparticles, the lipid moiety may not be sufficient to elicit interaction of the conjugated drug with plasma lipoproteins but the whole NP physicochemical features must be carefully considered.

Keywords: Lipoproteins, drug delivery, nanoparticles, lipid prodrugs, gemcitabine

1. Introduction

The ability of lipoproteins (LPs) to transport drugs has been described as early as 1981 (Counsell and Pohland, 1982; Firestone et al., 1984; Gal et al., 1981; Masquelier et al., 1986). Unlike most synthetic nanocarriers, LPs provide biocompatibility, biodegradability and non-immunogenicity (Thaxton et al., 2016). In addition, their structure makes them suitable for drug delivery thanks to: *(i)* a small size ranging from 5 nm (high-density lipoproteins (HDL)) to 100 nm (very low-density lipoproteins (VLDL)) preventing rapid clearance by the cells of the reticuloendothelial system, *(ii)* a hydrophobic core that could transport hydrophobic drugs, and *(iii)* a more hydrophilic outer envelope for amphiphilic molecules loading (Davis and Vance, 1996).

On the other hand, lipoproteins are attractive drug carriers to treat, at least theoretically, any pathological situation that implies their tissue accumulation, in particular neoplastic diseases. Indeed, due to higher cholesterol and cholesteryl esters requirements compared to healthy tissues, most tumors overexpress the low-density lipoprotein (LDL) receptor (LDLR) (Firestone, 1994; Vitols, 1991) and/or the HDL scavenger receptor type B1 (SR-B1) (Mooberry et al., 2016). Accordingly, along with the fact that VLDL and chylomicrons suffer from a low plasma half-life (Thaxton et al., 2016), LDL and HDL have been the predominant lipoproteins investigated for selective drug delivery to tumors (Mahmoudian et al., 2018). Applications in oncology have been largely documented in the past years, but similar strategies have been pursued to target other LP-accumulating tissues such as atherosclerotic plaques (Chen et al., 2020a; Tabas et al., 2007) or organs such as the brain (Chen et al., 2020b; Dehouck et al., 1997).

In this context, the *in vitro* loading of isolated lipoproteins with various drug molecules has been proposed. It includes conjugation of the drug to the apolipoprotein moieties, its insertion in the phospholipid outer layers or its encapsulation into the hydrophobic core of the LP (Zhu

and Xia, 2017). Lipoproteins can be obtained from fresh donor plasma through a variety of separation techniques according to their size, density or apolipoprotein content (*e.g.*, ultracentrifugation, gel permeation, size exclusion chromatography, affinity chromatography, immunocapture assays) (Busbee et al., 1981; Havel et al., 1955; Tadey and Purdy, 1995; Wasan et al., 1999; Watanabe et al., 2012). However, the need to isolate LP from fresh plasma is a major burden for their use in routine clinical practice. All these methods are indeed low yielding and time consuming, not to mention variations between plasma donors making batch reproducibility difficult. The inherent risk they pose in terms of blood contamination and LP denaturation during the disruptive extraction and loading processes represents another concern with this approach (Busatto et al., 2020).

Formulation of lipoprotein-like carriers has emerged as an alternative strategy. It relies on the *in vitro* assembly of commercially available lipids in proportions close to that found in natural lipoproteins, therefore bypassing the LP-harvesting step (Corbin and Zheng, 2007; Huang et al., 2015; Pittman et al., 1987). Going beyond simple mimicking, surface-functionalization of these artificial LPs with various ligands has even made it possible to reroute them from their natural pathways and promote their accumulation in target tissues overexpressing other specific receptors (Chen et al., 2007; Corbin et al., 2013; Han et al., 2020; Meng et al., 2015; Zhang et al., 2010; Zheng et al., 2005). Although promising, this approach remains quite laborious since it requires the opportune formulation of a variety of lipids (*i.e.*, phospholipids, cholesterol, cholesterol esters, triglycerides) and apolipoproteins. It also suffers from the fact that these apolipoproteins have to be extracted from human serum, and are difficult to handle because of their poor water-solubility and large size (Corbin and Zheng, 2007).

Overall, the complex production and storage of both the plasma-derived and the artificial lipoproteins, along with the aforementioned concerns, have hindered any industrial transposition and clinical application of LP-based drug delivery systems to date.

It is therefore evident that being able to trigger a drug-lipoprotein interaction directly in the blood circulation would be an easier way to exploit the natural transport capacity of lipoproteins.

We have recently discovered that the conjugation of gemcitabine, a hydrophilic anticancer drug, to the lipophilic squalene chain resulted in a preferential accumulation of the prodrug into lipoproteins, while the free drug did not show any affinity for the latter (Sobot et al., 2017a). Following this interaction, the LPs acted as indirect carriers transporting the squalene-gemcitabine (SQGem) prodrug toward high LP-accumulating cancer cells, leading to a higher therapeutic efficacy compared to free gemcitabine (Sobot et al., 2017b).

As lipoproteins are the natural transporters of cholesterol in the blood circulation, the question remains whether the conjugation of gemcitabine (as a model drug) to cholesterol could provide an even better interaction with endogenous lipoproteins.

Therefore, in the present study, we have explored the fate of nanoparticles (NPs) made of the cholesterol-gemcitabine (CholGem) conjugate both *in vitro* after incubation with human blood and *in vivo* after intravenous administration to rodents. Further information was then obtained by directly analyzing the interactions of these NPs with isolated blood components (*i.e.*, LDL, HDL, albumin). The conjugation to the cholesterol resulted in the formation of a prodrug and the activity of the gemcitabine is recovered only after its release from the conjugate following the *in vivo* enzymatic cleavage of the carbamate bond (Ghosh and Brindisi, 2015; Rautio et al., 2008). However, the assessment of a potential therapeutic activity of the CholGem NPs was not within the scope of this work, which was voluntarily focused on the evaluation of interactions with the components of biological media.

Altogether, these results contribute to shed light on what could drive the *in vivo* fate of NPs made of lipid prodrugs.

2. Materials and methods

2.1. Materials

Regular analytical grade and deuterated solvents were supplied by Carlo Erba (France) and Eurisotop (France), respectively. Tetrahydrofuran (THF) was distilled from sodium/benzophenone ketyl. Pyridine, triethylamine and dimethylformamide (DMF) were distilled from calcium hydride under a nitrogen atmosphere. All reactions involving air- or water-sensitive compounds were routinely conducted in glassware which was flame-dried under a positive pressure of nitrogen. Gemcitabine (Gem) base was purchased from Carbosynth Ltd (UK). Squalene (SQ), cholesteryl chloroformate, ethyl chloroformate, pyridine, triethylamine, sodium hydrogen carbonate, hydrogen chloride, sodium chloride and sodium bromide (NaBr) were purchased from Sigma-Aldrich (France). Chemicals obtained from commercial suppliers were used without further purification. Deionized and filtered MilliQ water was produced using a water purification system (Millipore, France).

2.2. Chemical characterization

Infrared spectra (IR) were obtained as solid or neat liquid on a Fourier transform Bruker Vector 22 spectrometer. Only significant absorptions are listed. Optical rotations were measured on a PerkinElmer 241 polarimeter at 589 nm. The ^{1}H and ^{13}C NMR spectra were recorded on a Bruker Avance 300 spectrometer (300 and 75 MHz for ^{1}H and ^{13}C, respectively). Recognition of methyl, methylene, methine, and quaternary carbon nuclei in ^{13}C NMR spectra rests on the *J*-modulated spin-echo sequence. Mass spectra (MS) and high resolution mass spectra (HRMS) were recorded using electrospray ionization (ESI) on an LTQ Velos Pro mass spectrometer (ThermoScientific, Germany). Analytical thin-layer chromatography was performed on Merck silica gel $60F_{254}$ glass pre-coated plates (0.25 mm layer). Column chromatography was performed on Merck silica gel 60 (230-400 mesh

ASTM). Semi-preparative high-performance liquid chromatography (HPLC) was performed using a Phenyl 5 µm XBridge Prep column 10 x 150 mm (PN 186003273, batch 121331521, Waters) with a cell Berthold YG50-S5P. Counting of radiolabeled prodrugs after synthesis was performed on a PerkinElmer Tricarb 2910 TR liquid scintillation analyzer equipped with automatic external standardization. Samples were prepared with the Ultima Gold^{TM} scintillation cocktail in 10 mL super polyethylene vials (PerkinElmer).

2.3. NP preparation and characterization

NPs were prepared by the nanoprecipitation solvent evaporation technique. Briefly, conjugates were dissolved at 2 mg.mL^{-1} in EtOH. The resulting organic solution (500 µL) was added dropwise to a stirred solution of MilliQ water (1 mL). The organic solvent was then removed under reduced pressure using a rotary evaporator to reach a 1 mg.mL^{-1} aqueous dispersion of NPs. ^{3}H-SQGem and ^{3}H-CholGem NPs were prepared in a similar manner. An appropriate volume of the radiolabeled conjugate was mixed with the cold one prior to the nanoprecipitation step in water, in order to obtain a NP dispersion with a final activity of 40 µCi.mL^{-1} and 50 µCi.mL^{-1} for *in vitro* and *in vivo* studies, respectively. Dextrose (5% m/v) was added to the final formulations to ensure isotonic conditions. The NP mean diameter was measured by dynamic light scattering with a Nano ZS (173° scattering angle, Malvern Panalytical, France) at 25 °C and monitored over a two-week period at room temperature. The zeta potential of NPs was measured at 25 °C after dilution with 1 mM NaCl solution by applying the Smoluchowski equation and using the same apparatus. All measurements were performed at least in triplicate.

2.4. Cryogenic transmission electron microscopy (cryo-TEM)

The morphology of SQGem and CholGem NPs was examined by cryo-TEM. Briefly, 5 µL of NP dispersion (1 $mg.mL^{-1}$) was deposited onto a 200-mesh holey carbon copper grid (TedPella Inc., USA) and flash-frozen in liquid ethane cooled at liquid nitrogen temperature. Cryo-TEM images were acquired on a JEOL 2200FS energy-filtered (20 eV) field emission gun electron microscope (JEOL, USA) operating at 200 kV using a Gatan ssCCD 2048 × 2048 pixels (Gatan Inc., USA).

2.5. Atomic force microscopy (AFM)

AFM experiments were performed in liquid conditions on mica substrates with surface area of 1.5 x 1.5 cm^2. Because of its plate-like structure, composed of an octahedral alumina sheet sandwiched by two tetrahedral silicate sheets, the cleavage of muscovite mica surface reveals a molecular smooth negatively charged surface. For experiments using pre-treated mica, the latter was immersed in a fresh 0.1 $g.L^{-1}$ poly-L-lysine aqueous solution for 30 min before rinsing with water. 1 mL of NP dispersion (10 $\mu g.mL^{-1}$ in MilliQ water) was deposited during 2 h onto the mica surface. AFM experiments were performed using the Nanowizard 3 Ultra Speed (JPK Instruments, Germany) installed on an air-buffered table coupled to a dynamic anti-vibration device and enclosed in an acoustic box. Imaging of the surface morphology was performed in water in Hyper Drive mode (JPK Instruments), with gold-coated silicon cantilever of 24 ± 0.5 $N.m^{-1}$ spring constant and 140 ± 2 kHz resonance frequency. The pyramid-shaped tips had a radius of curvature less than 20 nm. A free amplitude oscillation of 10 nm with 0.67 nm setpoint in amplitude and phase setpoints ranging between 0.9° and 1.2° was chosen, allowing the best resolution of the imaged surface. Images were taken at scan rate of 1 or 0.5 Hz for large scale pictures. Image processing (flatten, plane fit, edge, and hole

detection) was performed with the JPK Data Processing software (JPK Instruments). At least three different areas of each sample were scanned, and representative images are presented.

2.6. Surface Plasmon Resonance (SPR)

Interaction analyses were performed on a Biacore T100 instrument using CM5 Series S sensor chips (Cytiva, France). The activation of the carboxymethylated dextran matrix was performed with a 1/1 ratio mixture of 0.4 M N-ethyl-N'-(3-diethylaminopropyl)-carbodiimide (EDC)/0.1 M N-hydroxysuccinimide (NHS) (GE Healthcare, France) for 7 min. Solutions of either human serum albumin (HSA) (A3782, Sigma-Aldrich) or rat serum albumin (RSA) (A6414, Sigma-Aldrich) at 20 $\mu g.mL^{-1}$ in 10 mM acetate buffer (pH 4.5) were injected over the activated surface at 5 $\mu L.min^{-1}$ during 7 min. The average immobilization level was of 660 resonance units (RU) for HSA and 620 RU for RSA. A solution of ethanolamine hydrochloride (1 M, pH 8.5) was injected during 7 min to block the unreacted sites of the sensing surfaces. For reference, an additional blank flow channel was prepared in accordance with the same process but without injecting the albumin over the surface. Binding capacities of the functional surfaces were tested with 3 min injections at 10 $\mu L.min^{-1}$ of SQGem or CholGem NPs (concentration range: 17.5-560 µM in MilliQ water). An additional washing step with EtOH was added to prevent lipids from sticking to the fluidic system. After each cycle, the sensing surfaces were regenerated by injection of 70% EtOH (30 s, 30 $\mu L.min^{-1}$), followed by a 10 mM NaOH solution (60 s, 30 $\mu L.min^{-1}$). All experiments were carried out in duplicate at 37 °C in Dulbecco-Phosphate Buffered Saline (PBS) running buffer.

2.7. Plasma lipid and protein profile determination

Fresh citrated blood of healthy volunteers was obtained from the *Etablissement Français du Sang* (EFS, Paris, France, Agreement n°*17/EFS/031*). Lipid composition (total cholesterol,

triglycerides, LDL-C, HDL-C, ApoB, ApoA, Lip(a)) and albuminemia were assessed at the Georges Pompidou European Hospital (France) using standard laboratory procedures. Molar concentrations of LDL and HDL in the plasma of each blood bag were determined as previously reported (Sobot et al., 2017a) taking into account the molecular weight of LDL and HDL (2.3×10^6 and 1.8×10^5 Da respectively), and the percentage of apolipoprotein (Apo) present in each of them (21% of ApoB and 50% of ApoA in LDL and HDL, respectively) (Ohnishi et al., 2002). All blood samples had normal lipid and albumin concentrations.

2.8. Transmission electron microscopy (TEM)

A physical mixture of NP aqueous dispersion (final concentration 0.74 mM) and LPs in phosphate buffer (final concentration 0.1 µM) was incubated for 5 min at 37 °C in a thermoshaker (400 rpm) immediately before grid preparation. Five microliters of the mixture was then deposited on Formvar/carbon 400 mesh copper grid. After 5 min at room temperature, the remaining drop was blotted with a filter paper. Then, a drop of 0.22 µm-filtered 2% uranyl acetate solution was added for 30 s for negative staining and the excess of volume was removed with a blotting filter paper. The grids were then observed with a JEOL 1400 120 kV electron microscope operating at 80 kV at a nominal magnification of 5,000-40,000. Digital images were directly recorded on a CCD postcolumn high-resolution (11 MegaPixel) high-speed camera (SC1000 Orius, Gatan Inc.) using the Digital Micrograph image acquisition and processing software (Gatan Inc.). Images of isolated NPs (0.74 mM) and LP dispersion (0.1 µM) were acquired following the same protocol. All samples were prepared at a constant water/phosphate buffer ratio (57/1 v/v).

2.9. Incubation of radiolabeled NPs with human blood and LP separation

3.9 mL of whole human blood was incubated with 100 µL of ^{3}H-SQGem or ^{3}H-CholGem NPs (final volumetric activity in blood: 1 µCi.mL^{-1}, final NP concentration in blood: 39 µM and 37 µM for SQGem and CholGem, respectively) for 5 min at 37 °C. Following a first centrifugation step to remove the red blood cells (3,000 *g*, 15 min, 15 °C), plasma components were separated by NaBr gradient density ultracentrifugation (Cassidy et al., 1998; Sobot et al., 2017a). All NaBr solutions and plasma were cooled at 4 °C for 1 h prior to ultracentrifuge tube preparation. 1 mL of 1.006 g.mL^{-1} NaBr solution was placed at the bottom of a 4 mL Ultraclear ultracentrifuge tube (344062, Beckman Coulter), and was then underlaid with 1 mL of increasing density NaBr solutions (1.063 and 1.21 g.mL^{-1}). Finally, 1 mL of plasma, whose density was adjusted to 1.25 g.mL^{-1} with NaBr, was carefully added at the bottom of the tube. The tubes were placed on a SW 60Ti swinging bucket rotor (Beckman Coulter) and ultracentrifuged (164,326 *g*, 18 h, 15 °C) using an Optima™ LE-80K Ultracentrifuge (Beckman Coulter). At the end of the centrifugation cycle, twenty fractions of 200 µL each were collected from the top to the bottom of the tube using single use 1 mL insulin syringes (324891, BD). The density of each fraction was then measured, and the radioactivity counted.

2.10. Radioactivity measurements

100 µL of each fraction was mixed to 10 mL of Ultima Gold™ scintillation cocktail (6013329, PerkinElmer) in scintillation vials. Samples were vortexed vigorously for 30 s and kept aside for 1 h before radioactivity measurement using a β-scintillation counter (LS6500, Beckman Coulter).

2.11. Dialysis of separated fractions from human plasma

Prior to electrophoresis and cholesterol and albumin dosages, the collected plasma fractions were dialyzed against a Tris-buffered saline solution (50 mM Tris, 150 mM NaCl, pH 7.4) for 2 h using 3.5 kDa MWCO Slide-A-Lyzer™ MINI dialysis devices (10321114, Fisher Scientific). Buffer was changed every 30 min. The dilution factor was determined by measuring the volume of each fraction before and after the dialysis step.

2.12. Electrophoresis

The quality of the LP separation was assessed by electrophoresis using the HYDRAGEL LIPO + Lp(a) K20 separation kit (3007, SEBIA). Following the manufacturer instructions, 10 µL of each dialyzed fraction was loaded onto the agarose gels and allowed to migrate at a constant voltage of 50 V for 90 min. Then, gels were dried at 80 °C for at least 45 min, stained with Sudan Black, bleached and washed with the supplied reagents. The LP identity within each fraction was confirmed by the migration distance of the electrophoretic bands from the loading point.

2.13. Cholesterol and albumin dosage

Cholesterol and albumin content in each plasma fraction was quantified using the cholesterol assay kit (ab65390, Abcam) and the human albumin ELISA kit (ab227933, Abcam), according to the provider instructions.

2.14. Animals

Male Sprague Dawley rats (4-week-old) were bought from Janvier Labs (France). All animals were housed in appropriate animal care facilities during the experimental period and were handled according to the principles of laboratory animal care and legislation in force in

France. Experimental approval was obtained from the Ethical Committee C2EA-26 (Authorization number *#3805.02*).

2.15. In vivo ^{3}H-SQGem and ^{3}H-CholGem NPs administration to rats and LP separation

Radiolabeled ^{3}H-SQGem and ^{3}H-CholGem NPs (1.0 mg.kg^{-1} eq. Gem, 20 µCi *per* rat) were administered to healthy male Sprague Dawley rats by intravenous injection in the tail vein. After 5 min, blood was collected by cardiac puncture into EDTA K_3 Vacuette tubes (VK054STK, Labelians). Rats were kept under anesthesia with a mixture of ketamine (100 mg.kg^{-1}) and xylazine (10 mg.kg^{-1}) during the whole process. The separation protocol was performed in a similar manner as in the *in vitro* assay on human blood with small adjustments to best fit the murine model. Following a first centrifugation of the blood (1,700 *g*, 15 min, 15 °C), plasma was separated by sodium bromide gradient density ultracentrifugation using NaBr solutions of 1.006, 1.054 and 1.210 g.mL^{-1} densities which have been chosen to match those of the different LP populations in rodents. Afterwards, separation was performed as described above (*see 2.9.*).

3. Results and discussion

3.1. NP formulation and physicochemical characterization

As for the SQGem prodrug (Fig. 1a), the cholesterol moiety has also been conjugated to the amino group of gemcitabine (Fig. 1c), allowing protection of the drug from the metabolization by plasma deaminases (Couvreur et al., 2006). Radiolabeled conjugates were synthesized in a similar manner, using a ^{3}H-Gem radiolabeled in the position C-5 of the cytosine moiety (Fig. 1b, d).

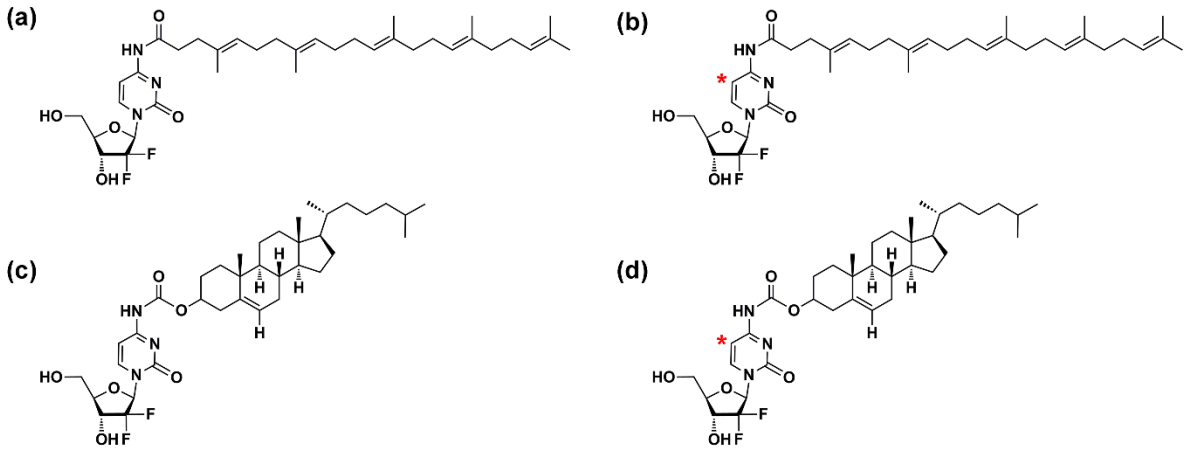

Fig. 1. Chemical structures of (a) squalene-gemcitabine (SQGem) and (c) cholesterol-gemcitabine (CholGem) prodrugs and their tritiated equivalent (b) ^{3}H-SQGem and (d) ^{3}H-CholGem (*, site of ^{3}H incorporation).

The nanoprecipitation of CholGem prodrugs resulted in their self-assembly into nanoparticles with a mean diameter of 97 nm, a narrow size distribution and a negative surface charge of -21 mV, similar to SQGem NPs, herein used as a well-characterized reference. However, CholGem NPs showed almost a three-fold longer stability at room temperature, comparatively to SQGem NPs which displayed visible aggregates from day 7 (Fig. 2c). Only a slight decrease in size occurred when the radiolabeled ^{3}H-CholGem prodrug was introduced in the formulation (Table 1).

Table 1

SQGem and CholGem nanoparticle characterization.

Conjugate	Mean diameter[a] (nm)	Polydispersity index[a] (PdI)	Zeta Potential[a] (mV)	Drug loading[b] (%)
SQGem	82 ± 7	0.11 ± 0.03	-20 ± 7	40.7
CholGem	97 ± 15	0.09 ± 0.02	-21 ± 7	38.9
^{3}H-SQGem	86 ± 5	0.15 ± 0.02	-	-
^{3}H-CholGem	77 ± 10	0.10 ± 0.04	-	-

[a] Measured by dynamic light scattering (values ± standard deviation, n ≥ 15).
[b] Calculated as molecular weight (gemcitabine)/molecular weight (conjugate).

Both SQGem and CholGem NPs displayed spherical structures (Fig. 2a, b) but cryo-TEM images revealed a different supramolecular organization, the CholGem NPs assembling as vesicle-like structures (Fig. 2b). The latter showed a highly contrasted envelope likely corresponding to a bilayer made of amphiphilic CholGem prodrugs and stabilized by hydrophobic interactions between the cholesterol moieties.

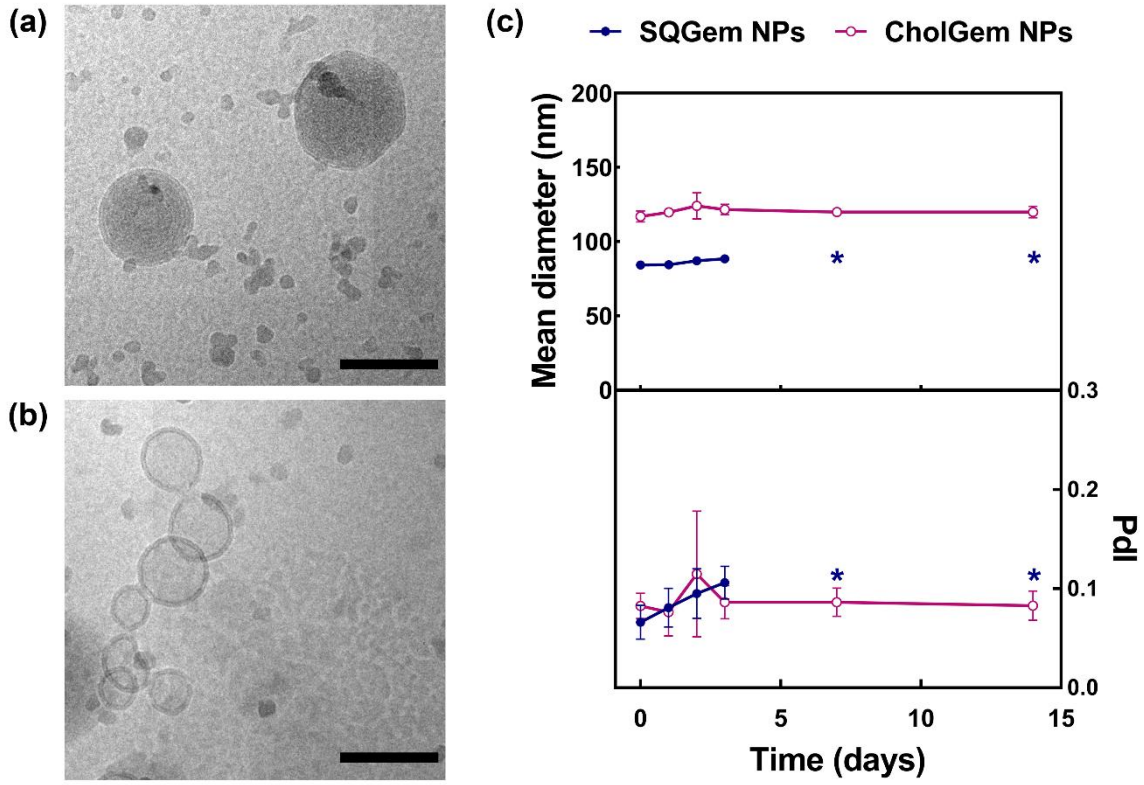

Fig. 2. Cryo-TEM images of (a) SQGem NPs (1 mg.mL^{-1}) and (b) CholGem NPs (1 mg.mL^{-1}), scale bar: 100 nm; (c) evolution of NP mean diameter and polydispersity index (PdI) in water during storage at room temperature. (*: visible aggregates in the sample). Values represents mean ± standard deviation (n=3).

3.2. In vitro distribution of ^{3}H-SQGem and ^{3}H-CholGem in human plasma

The distribution of SQGem and CholGem prodrugs within the plasma fractions has been first investigated *in vitro* following incubation with whole human blood at 37 °C for 5 min. After sodium bromide gradient density ultracentrifugation, twenty plasma fractions were isolated (numbered from top to bottom of the tube). According to their electrophoretic profile (Fig. S9b), their density (Fig. S12a) and their cholesterol content (Fig. 3), these fractions were attributed to the different lipoprotein subclasses: *(i)* VLDL: fraction 1, *(ii)* LDL: fractions 2-5, *(iii)* HDL: fractions 7-13 and *(iv)* to the lipoprotein deficient fraction (LPDF: fractions 14-19) in which albumin accumulated (Fig. S9a and Fig. S11). A small pellet was present in fraction 20 which likely corresponded to lipoprotein residues and cellular debris.

Prodrug content in these fractions was determined by radioactivity quantification which was then normalized to the radioactivity in plasma. SQGem NPs have been herein used as a reference and, in agreement with the previous data (Sobot et al., 2017a), a main accumulation in the cholesterol-rich lipoprotein fractions was detected. On the contrary, CholGem was only detected in the lipoprotein-deficient fractions at the bottom of the tube and not in the LP fractions (Fig. 3). Of note, the higher variability of the CholGem results among replicates compared to the more reproducible distribution profile of SQGem NPs, suggested the absence of any association of CholGem with plasma components and a rather nonspecific partition at the bottom of the ultracentrifugation tubes.

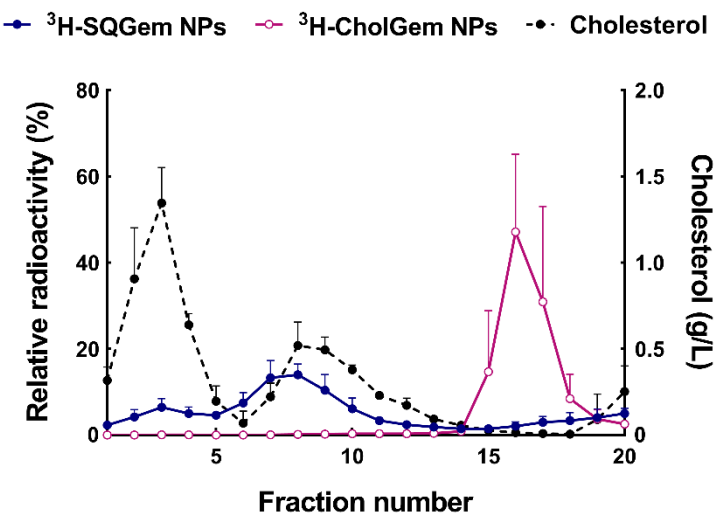

Fig. 3. Distribution of ^{3}H-SQGem, ^{3}H-CholGem and endogenous cholesterol among the plasma fractions collected after NP incubation in whole human blood. Results are expressed as relative radioactivity % (mean values) compared to total plasma. Error bars correspond to standard deviation (^{3}H-SQGem NPs n=6; ^{3}H-CholGem NPs n=6; Cholesterol n=3).

3.3. In vivo distribution of ^{3}H-SQGem and ^{3}H-CholGem in rat plasma

We additionally investigated whether a similar plasma distribution of CholGem NPs also occurred *in vivo* upon intravenous administration of NPs to rats. *In vivo* studies were carried out with the radiolabeled NPs for better detection sensitivity. 5 min after the injection of ^{3}H-SQGem or ^{3}H-CholGem NPs, the blood was collected by cardiac puncture and the plasma fraction separation was carried out as described above.

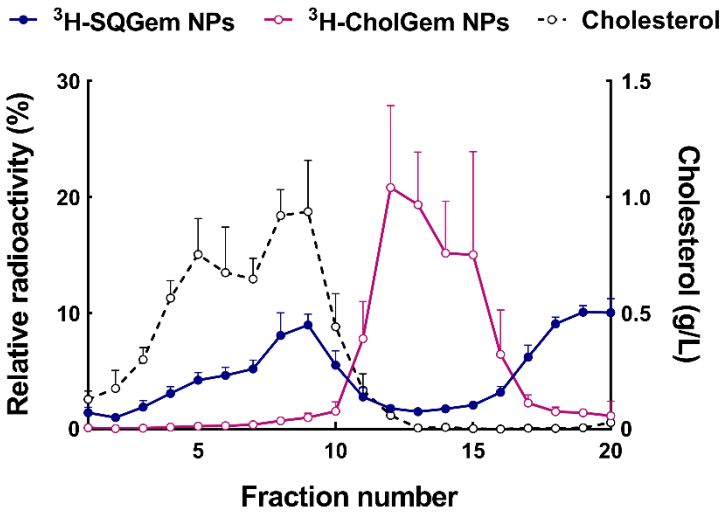

Fig. 4. Distribution of ^{3}H-SQGem, ^{3}H-CholGem and endogenous cholesterol among the plasma fractions collected after NP intravenous administration to rats. Results are expressed as relative radioactivity % (mean values) compared to total plasma. Error bars correspond to standard deviation (^{3}H-SQGem NPs n=6; ^{3}H-CholGem NPs n=7; Cholesterol n=4).

The *in vivo* blood distribution profile of the two types of NPs closely resembled to that observed *in vitro*. Now again, the SQGem was recovered in the cholesterol-rich LP 1-13 fractions, while the level of CholGem in the different fractions was opposite and inversely proportional to their content in endogenous cholesterol (Fig. 4).

Of note, electrophoretic mobility (Fig. S10b) and density profile (Fig. S12b) revealed a similar LP distribution among the fractions compared to the one found in human plasma (*i.e.*, VLDL: fractions 1-2, LDL: fractions 1-5, HDL: fractions 3-13 and LPDF: fractions 14-20). Yet, the distribution of cholesterol between the LP classes *in vivo* (Fig. 4, Fig. S11) differed from those observed *in vitro* (Fig. 3, Fig. S11), reflecting the different lipoprotein metabolism in humans and rodents and confirming the role of HDL as main cholesterol carrier in the latter (Camus et al., 1983; Innerarity et al., 1980; Oschry and Eisenberg, 1982).

As also observed for human samples, the gradient ultracentrifugation of rat plasma led to albumin accumulation in the LP-deficient 16-20 fractions (Fig. S10a, S11). *In vitro,* in human blood, the CholGem profile partially overlapped the albumin distribution (Fig. S9a), while *in vivo* in rats the two traces were clearly separated (Fig. S10a). In these LP-deficient fractions, the cumulated amount of the SQGem conjugate reached around 18% of the total radioactivity in human plasma (Fig. S9a) and was twice as high in rodent plasma (39%) (Fig. S10a). Whether such different trend was related to a different affinity toward the human or rat serum albumin deserved to be further investigated.

3.4. Interaction of SQGem and CholGem NPs with serum albumin

The affinity of SQGem and CholGem NPs for both human serum albumin (HSA) and rat serum albumin (RSA) was thus assessed by SPR. HSA and RSA were fixed onto separate flow channels of a CM5 chip, and SQGem and CholGem NPs were injected at different concentrations (Fig. 5).

For both HSA and RSA (Fig. 5a, c), SQGem NPs injections resulted in a concentration-dependent response which supported SQGem affinity for albumin, in agreement with previous *in silico* studies (Yesylevskyy et al., 2018). Signal amplitude was slightly higher for the couple SQGem NPs/RSA (Fig. 5c) compared to the SQGem NPs/HSA (Fig. 5a), which may explain the different quantities of SQGem detected in the albumin-rich fractions when NPs entered into contact with human (Fig. S9a) or rat blood (Fig. S10a).

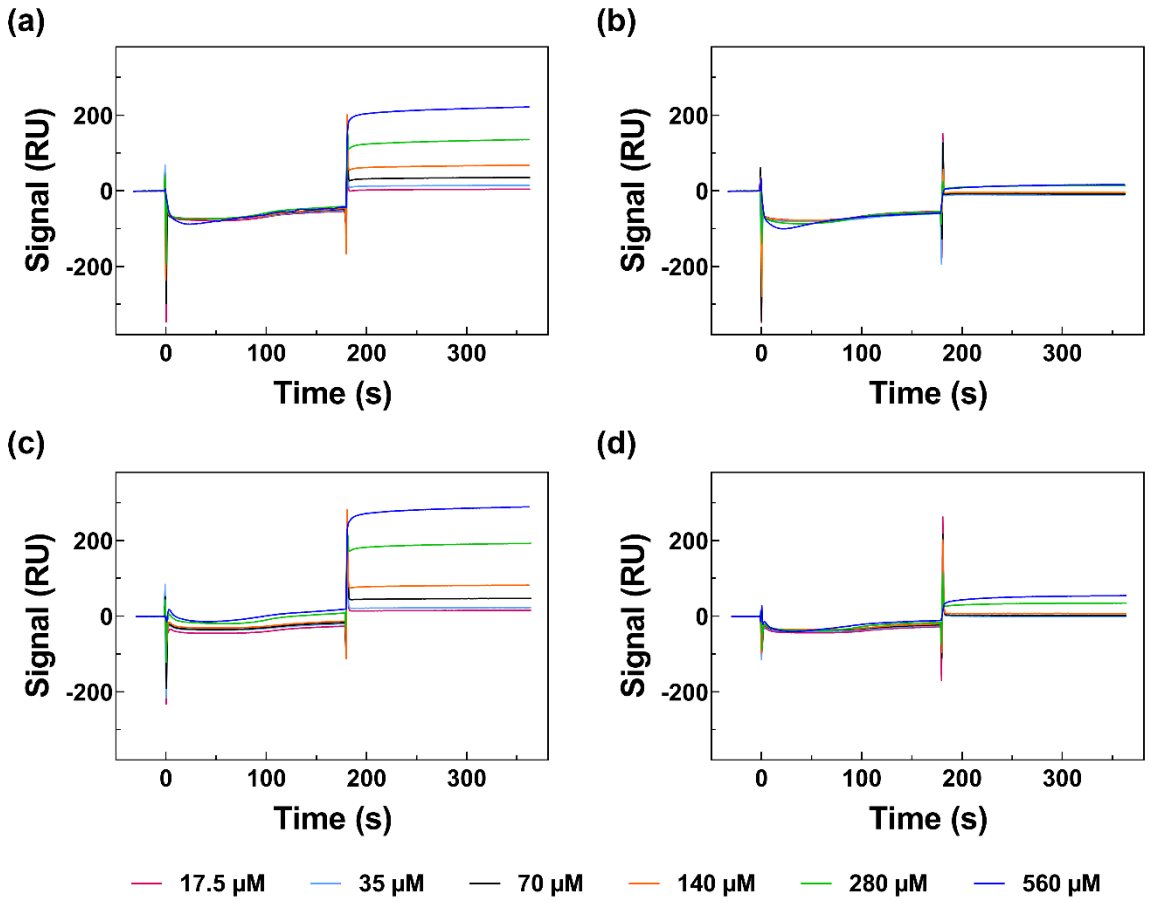

Fig. 5. Reference-subtracted SPR sensorgrams (resonance units (RU) versus time) obtained by injection of (a, c) SQGem NPs and (b, d) CholGem NPs over (a, b) human or (c, d) rat albumin, immobilized on a CM5 sensor chip.

On the contrary, the interaction of CholGem NPs with rat or human albumin was almost inexistent (Fig. 5b, d). Indeed, injection of these NPs at the highest concentrations (*i.e.*, 280 µM and 560 µM) in the channel containing HSA resulted in a signal almost ten times lower in amplitude than the one measured for the SQGem NPs at the same concentration (Fig. 5b). Similarly, when CholGem NPs were introduced in the RSA channel at concentrations above 140 µM, a concentration dependent trend appeared, but again the signal intensity was very weak, (*i.e.*, 6-times lower than the one observed with SQGem NPs), which did not validate a significant interaction, too (Fig. 5d).

Taken together with the *in vivo* and *in vitro* plasma distribution profiles (Fig. 3, 4), these results confirmed the capacity of SQGem NPs to interact with albumin in addition to lipoproteins. On the contrary, the presence of CholGem in some albumin-containing plasma fractions could not be correlated with any interaction between the two components.

3.5. Analysis of NP morphology by AFM

AFM analysis of SQGem and CholGem NPs has been carried out to ascertain whether differences in their respective behavior toward plasma components could (or not) be attributed to structural differences between them.

Both nanoparticles, which displayed a negative surface charge (Table 1), did not adsorb on an untreated negatively-charged mica surface (Fig. S13) but rapidly adhered to a lysine-coated positively-charged surface (Fig. 6) therefore revealing an attractive electrostatic-driven adsorption. The deposition of SQGem NPs onto the latter quickly led to the formation of 4 nm-height patches which spread out unevenly. This effect was likely due to their physisorption onto the surface, followed by a disruption of their supramolecular structure (Fig. 6a, b). On the contrary, heights from 20 to 40 nm were measured for the CholGem NPs suggesting that these 100 nm NPs flattened upon adsorption onto the surface but did not break (Fig. 6c, d). These results further suggested a difference in NP supramolecular organization: the squalene prodrug assembled in easily deformable NPs while the cholesterol derivatives led to stiffer NPs which prevented their rupture on the positively-charged mica surface.

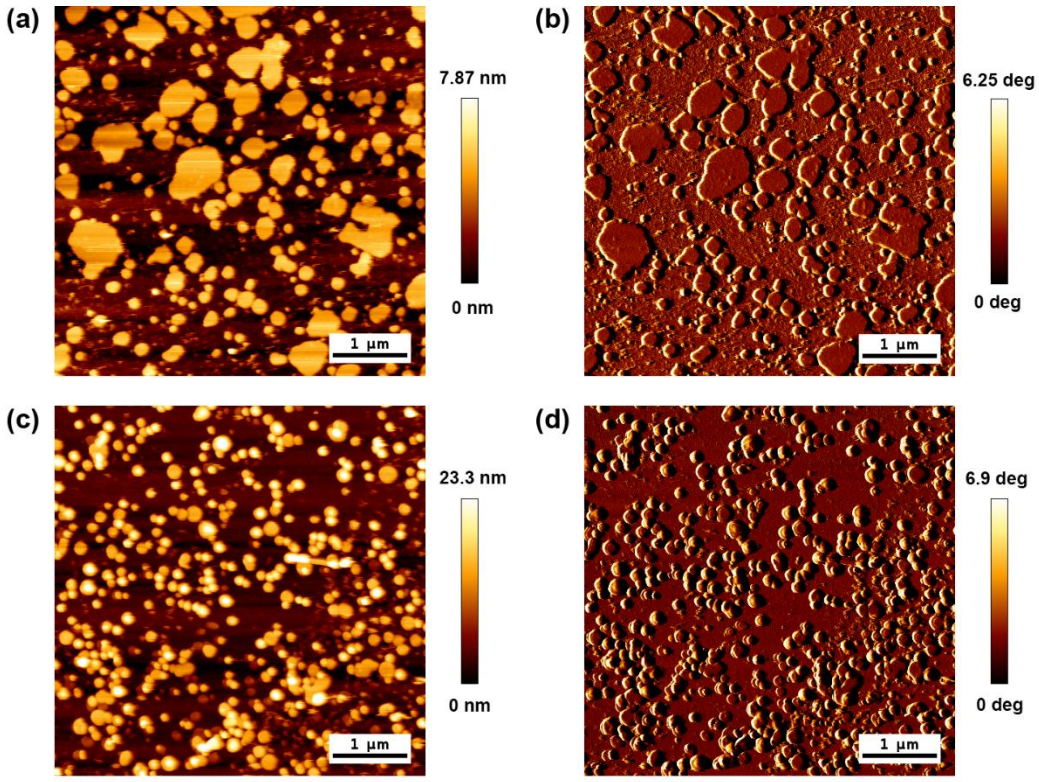

Fig. 6. AFM images obtained in liquid medium of (a, b) SQGem NPs and (c, d) CholGem NPs on mica surface previously treated with poly-L-lysine. (a, c) Height images, (b, d) phase images.

3.6. TEM observations of NP/ lipoprotein mixtures

The likely more stable and rigid structure of the CholGem NPs has been confirmed qualitatively by TEM observations in the presence of isolated lipoproteins (Fig. 7). Upon physical mixture with LDL (Fig. 7e) or HDL (Fig. 7g) a merge of SQGem NPs and lipoproteins was observed, probably triggering the previously described disassembly of these nanoparticles resulting from the insertion of SQGem as single molecular entities into the lipoprotein core (Cayre et al., 2017; Sobot et al., 2017a). On the contrary, CholGem NPs coexisted with either LDL (Fig. 7f) or HDL (Fig. 7h) without any apparent interaction as suggested by the lack of modification of their well-defined bilayer. These NPs tended to stick together and to form large clusters independently of the presence of lipoproteins.

Further imaging of the same mixtures after a 19 h incubation period revealed the greater deformation of SQGem NPs in presence of LPs in comparison to CholGem in the same conditions (Fig. S14).

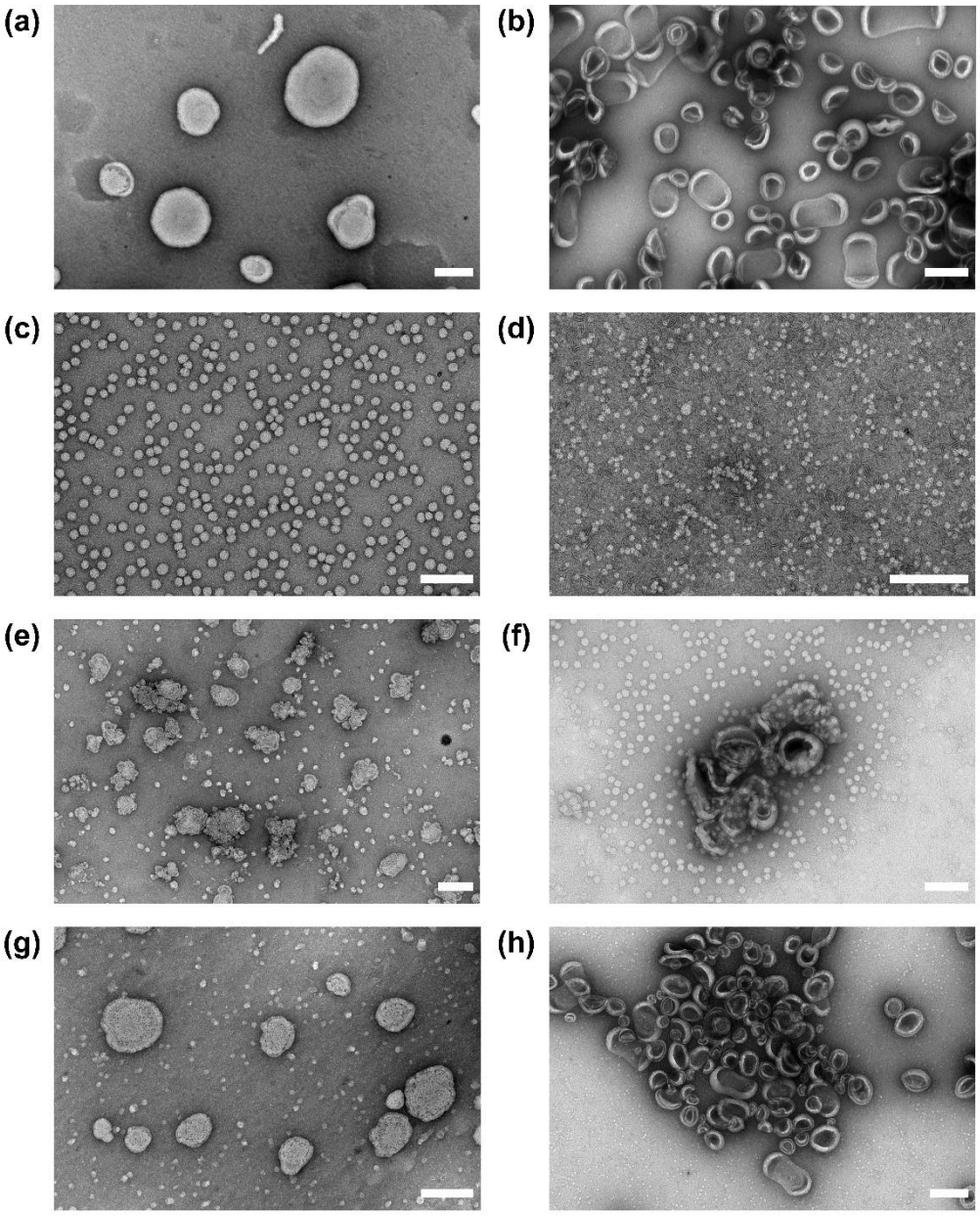

Fig. 7. TEM images of (a) SQGem NPs, (b) CholGem NPs, (c) LDL, (d) HDL and physical mixtures of (e) SQGem NPs and LDL, (f) CholGem NPs and LDL, (g) SQGem NPs and HDL, (h) CholGem NPs and HDL. Scale bar: 200 nm. Final concentrations of NPs and lipoproteins (LDL or HDL) were of 0.74 mM and 0.1 µM, respectively. All samples were incubated for 5 min at 37 °C prior to observation.

Altogether, AFM and TEM observations pointed toward a more fragile nature of the SQGem NPs that could explain their easier disassembly in biological conditions and their interaction with lipoproteins with subsequent transfer of SQGem molecules into the LP core. On the contrary, the CholGem NPs were more stable and maintained their structural integrity over time, limiting interactions with blood components (both LPs and albumin).

4. Conclusion

Aiming to exploit endogenous lipoproteins for selective drug delivery to neoplastic tissues, we have herein investigated whether the drug conjugation to a LP component, like cholesterol, could have been a sufficient condition. Using gemcitabine as a model drug, we have conjugated this anticancer compound to cholesterol, because it is one of the main lipids transported by LPs. The resulting amphiphilic conjugate was capable to self-assemble as nanoparticles. But, unexpectedly, no interaction with any lipoprotein fraction could be detected neither *in vitro* after incubation with human blood nor *in vivo* after intravenous administration to rats. Comparison with SQGem NPs, which clearly interacted with LPs, highlighted that other key parameter than the prodrug lipophilicity and the natural affinity of the lipid moiety for endogenous lipoproteins were involved in the prodrug interaction with LPs.

And, it was discovered that the structure of the NPs formed by the gemcitabine prodrug supramolecular assembly played a key role in the sequence of events occurring in the blood, the first biological medium encountered after NPs intravenous administration. Electron microscopy and atomic force microscopy experiments suggested, in comparison to CholGem, a much higher deformability of SQGem NPs and their modification over time in the presence of plasma components.

It remains an open question whether the physical constants of the lipid moieties can affect the properties of the prodrug nanoparticles, namely their rigidity, and thus the behavior of the NPs in the biological media. Cholesterol has a crystal structure and a higher melting point (148.2 °C) compared to squalene, an oil with a melting point of -4.5 °C (Haynes, 2016). Since conjugation of squalene and cholesterol to the gemcitabine resulted in prodrugs whose physical form closely resembled that of the parent lipid (an oily product (SQGem) and a solid powder (CholGem)) these two prodrugs are expected to have very distinct melting points. It can be speculated that the higher the melting point, the stronger the intermolecular interactions and thus the molecular packing, as previously observed for binary crystals (Kilinkissa et al., 2020).

Although further studies are needed to validate such a hypothesis, a trend might exist since in our study we showed that the lipid moiety with the lowest melting point (*i.e.*, squalene) led to nanoparticles with lower colloidal stability in the biological medium.

On the contrary, the lack of interaction with the plasma fractions suggests that the cholesterol moiety triggered the formation of more closely packed nanoparticles and conferred greater resistance to destabilization. This is in agreement with previous studies that demonstrated a crucial role of cholesterol in decreasing permeability of unsaturated phospholipid vesicles, increasing the packing density of phospholipid molecules in liposomes, and increasing the colloidal stability of these vesicles in the presence of blood components (Allen, 1981; Demel and De Kruyff, 1976; Kirby et al., 1980; Papahadjopoulos et al., 1973; Patel et al., 1983).

As the interaction of CholGem or SQGem prodrugs with LPs is likely to happen at the molecular scale, the nanoparticle destabilization upon injection might be a crucial prerequisite for the interaction to occur. In that respect, it is obvious that colloidal stable NPs such as CholGem are less prone to interact with endogenous lipoproteins.

Overall, these results point out that the interplay between the physicochemical properties of the prodrugs and the resulting supramolecular assembly as nanoparticles may strongly influence the fate of the conjugates in the bloodstream, further affecting pharmacological and toxicological properties.

Acknowledgments

This work was supported by the French Ministry of Research, the CNRS, the Fondation pour la Recherche Médicale (*Application FDT202001010776*) and the Ligue contre le Cancer (*Subvention Recherche HB2019-22 and NH2020-32*). It has benefited from the Imagerie- Gif core facility supported by l'Agence Nationale de la Recherche (ANR-11-EQPX-0029/Morphoscope, ANR-10-INBS-04/FranceBioImaging; ANR-11-IDEX-0003-02/ Saclay Plant Sciences), the Electron Microscopy Facility of the Multimodal Imaging Centre at Institut Curie, Orsay and the INTERMOL molecular interactions platform of the IPSIT/US31/UMS3679. We thank Miss Claire Boulogne and Miss Cynthia Gillet (Imagerie-Gif) for their assistance during the TEM experiments, Miss Assia Hessani (Institut Galien Paris-Saclay, France) for her help with radiolabeled materials, and Dr Sylvain Trépout (Institut Curie, France) for the cryo-TEM images. G.P. and S.F. thank ANR for funding T.N. (Carb2zyme, ANR- 17- CE11- 0014).

Appendix A. Supplementary information

Supplementary information to this article can be found online at xxx.

NMR spectra; radio-HPLC chromatograms and elution conditions; absorbance calibration curves used to determine radiolabeled products concentration; albumin distribution among human and rat plasma fractions; electrophoresis of human and rat plasma fractions; AFM images of SQGem and CholGem NPs on bare mica surface; TEM images of isolated NPs, LPs, and their physical mixtures after 19 h incubation at 37 °C.

References

Allen, T.M., 1981. A study of phospholipid interactions between high-density lipoproteins and small unilamellar vesicles. Biochim. Biophys. Acta 640, 385-397.

Busatto, S., Walker, S.A., Grayson, W., Pham, A., Tian, M., Nesto, N., Barklund, J., Wolfram, J., 2020. Lipoprotein-based drug delivery. Adv. Drug Deliv. Rev. 159, 377-390.

Busbee, D.L., Payne, D.M., Jasheway, D.W., Carlisle, S., Lacko, A.G., 1981. Separation and detection of lipoproteins in human serum by use of size-exclusion liquid chromatography: a preliminary report. Clin. Chem. 27, 2052-2058.

Camus, M.C., Chapman, M.J., Forgez, P., Laplaud, P.M., 1983. Distribution and characterization of the serum lipoproteins and apoproteins in the mouse, Mus musculus. J. Lipid Res. 24, 1210-1228.

Cassidy, S.M., Strobel, F.W., Wasan, K.M., 1998. Plasma lipoprotein distribution of liposomal nystatin is influenced by protein content of high-density lipoproteins. Antimicrob. Agents Chemother. 42, 1878-1888.

Cayre, F., Mura, S., Andreiuk, B., Sobot, D., Gouazou, S., Desmaele, D., Klymchenko, A., Couvreur, P., 2017. In Vivo FRET Imaging to Predict the Risk Associated with Hepatic Accumulation of Squalene-Based Prodrug Nanoparticles. Adv. Healthc. Mater. 7, 1700830.

Chen, J., Corbin, I.R., Li, H., Cao, W., Glickson, J.D., Zheng, G., 2007. Ligand Conjugated Low-Density Lipoprotein Nanoparticles for Enhanced Optical Cancer Imaging in Vivo. J. Am. Chem. Soc. 129, 5798-5799.

Chen, J., Zhang, X., Millican, R., Creutzmann, J.E., Martin, S., Jun, H.-W., 2020a. High density lipoprotein mimicking nanoparticles for atherosclerosis. Nano Converg. 7, 6.

Chen, Y.-x., Wei, C.-x., Lyu, Y.-q., Chen, H.-z., Jiang, G., Gao, X.-l., 2020b. Biomimetic drug-delivery systems for the management of brain diseases. Biomater. Sci. 8, 1073-1088.

Corbin, I.R., Ng, K.K., Ding, L., Jurisicova, A., Zheng, G., 2013. Near-infrared fluorescent imaging of metastatic ovarian cancer using folate receptor-targeted high-density lipoprotein nanocarriers. Nanomedicine (Lond) 8, 875-890.

Corbin, I.R., Zheng, G., 2007. Mimicking nature's nanocarrier: synthetic low-density lipoprotein-like nanoparticles for cancer-drug delivery. Nanomedicine (Lond) 2, 375-380.

Counsell, R.E., Pohland, R.C., 1982. Lipoproteins as potential site-specific delivery systems for diagnostic and therapeutic agents. J. Med. Chem. 25, 1115-1120.

Couvreur, P., Stella, B., Reddy, L.H., Hillaireau, H., Dubernet, C., Desmaële, D., Lepêtre-Mouelhi, S., Rocco, F., Dereuddre-Bosquet, N., Clayette, P., et al., 2006. Squalenoyl Nanomedicines as Potential Therapeutics. Nano Lett. 6, 2544-2548.

Davis, R.A., Vance, J.E., 1996. Chapter 17 - Structure, assembly and secretion of lipoproteins, in: Vance, D.E., Vance, J.E. (Eds.), Biochemistry of Lipids, Lipoproteins and Membranes. Elsevier, New York, NY, pp. 473-493.

Dehouck, B., Fenart, L., Dehouck, M.P., Pierce, A., Torpier, G., Cecchelli, R., 1997. A new function for the LDL receptor: transcytosis of LDL across the blood-brain barrier. J. Cell Biol. 138, 877-889.

Demel, R.A., De Kruyff, B., 1976. The function of sterols in membranes. Biochim. Biophys. Acta 457, 109-132.

Firestone, R.A., 1994. Low-density lipoprotein as a vehicle for targeting antitumor compounds to cancer cells. Bioconjug. Chem. 5, 105-113.

Firestone, R.A., Pisano, J.M., Falck, J.R., McPhaul, M.M., Krieger, M., 1984. Selective delivery of cytotoxic compounds to cells by the LDL pathway. J. Med. Chem. 27, 1037-1043.

Gal, D., Ohashi, M., MacDonald, P.C., Buchsbaum, H.J., Simpson, E.R., 1981. Low-density lipoprotein as a potential vehicle for chemotherapeutic agents and radionucleotides in the management of gynecologic neoplasms. Am. J. Obstet. Gynecol. 139, 877-885.

Ghosh, A.K., Brindisi, M., 2015. Organic Carbamates in Drug Design and Medicinal Chemistry. J Med. Chem. 58, 2895-2940.

Han, M., Ji, X., Li, J., Ge, Z., Luo, B., Zhou, K., Wang, Q., Sun, X., Zhang, W., Li, J., 2020. Lipoprotein-Inspired Nanocarrier Composed of Folic Acid-Modified Protein and Lipids: Preparation and Evaluation of Tumor-Targeting Effect. Int. J. Nanomedicine 15, 3433-3445.

Havel, R.J., Eder, H.A., Bragdon, J.H., 1955. The distribution and chemical composition of ultracentrifugally separated lipoproteins in human serum. J. Clin. Invest. 34, 1345-1353.

Haynes, W.M., 2016. CRC Handbook of Chemistry and Physics. 97th Edition. CRC Press, Boca Raton: FL 33487-2742.

Huang, H., Cruz, W., Chen, J., Zheng, G., 2015. Learning from biology: synthetic lipoproteins for drug delivery. Wiley Interdiscip. Rev. Nanomed. Nanobiotechnol. 7, 298-314.

Innerarity, T.L., Pitas, R.E., Mahley, R.W., 1980. Disparities in the interaction of rat and human lipoproteins with cultured rat fibroblasts and smooth muscle cells. Requirements for homology for receptor binding activity. J. Biol. Chem. 255, 11163-11172.

Kilinkissa, O.E.Y., Govender, K.K., Báthori, N.B., 2020. Melting point–solubility–structure correlations in chiral and racemic model cocrystals. CrystEngComm 22, 2766-2771.

Kirby, C., Clarke, J., Gregoriadis, G., 1980. Effect of the cholesterol content of small unilamellar liposomes on their stability in vivo and in vitro. Biochem. J. 186, 591-598.

Mahmoudian, M., Salatin, S., Khosroushahi, A.Y., 2018. Natural low- and high-density lipoproteins as mighty bio-nanocarriers for anticancer drug delivery. Cancer Chemother. Pharmacol. 82, 371-382.

Masquelier, M., Vitols, S., Peterson, C., 1986. Low-density lipoprotein as a carrier of antitumoral drugs: in vivo fate of drug-human low-density lipoprotein complexes in mice. Cancer Res. 46, 3842-3847.

Meng, F., Asghar, S., Gao, S., Su, Z., Song, J., Huo, M., Meng, W., Ping, Q., Xiao, Y., 2015. A novel LDL-mimic nanocarrier for the targeted delivery of curcumin into the brain to treat Alzheimer's disease. Colloids Surf. B Biointerfaces 134, 88-97.

Mooberry, L.K., Sabnis, N.A., Panchoo, M., Nagarajan, B., Lacko, A.G., 2016. Targeting the SR-B1 Receptor as a Gateway for Cancer Therapy and Imaging. Front. Pharmacol. 7, 466.

Ohnishi, T., Mohamed, N.A.L., Shibukawa, A., Kuroda, Y., Nakagawa, T., El Gizawy, S., Askal, H.F., El Kommos, M.E., 2002. Frontal analysis of drug–plasma lipoprotein binding using capillary electrophoresis. J. Pharm. Biomed. Anal. 27, 607-614.

Oschry, Y., Eisenberg, S., 1982. Rat plasma lipoproteins: re-evaluation of a lipoprotein system in an animal devoid of cholesteryl ester transfer activity. J. Lipid Res. 23, 1099-1106.

Papahadjopoulos, D., Jacobson, K., Nir, S., Isac, I., 1973. Phase transitions in phospholipid vesicles Fluorescence polarization and permeability measurements concerning the effect of temperature and cholesterol. Biochim. Biophys. Acta Biomembr. 311, 330-348.

Patel, H.M., Tuzel, N.S., Ryman, B.E., 1983. Inhibitory effect of cholesterol on the uptake of liposomes by liver and spleen. Biochim. Biophys. Acta 761, 142-151.

Pittman, R.C., Glass, C.K., Atkinson, D., Small, D.M., 1987. Synthetic high density lipoprotein particles. Application to studies of the apoprotein specificity for selective uptake of cholesterol esters. J. Biol. Chem. 262, 2435-2442.

Rautio, J., Kumpulainen, H., Heimbach, T., Oliyai, R., Oh, D., Järvinen, T., Savolainen, J., 2008. Prodrugs: design and clinical applications. Nat. Rev. Drug Discov. 7, 255-270.

Sobot, D., Mura, S., Yesylevskyy, S.O., Dalbin, L., Cayre, F., Bort, G., Mougin, J., Desmaele, D., Lepetre-Mouelhi, S., Pieters, G., et al., 2017a. Conjugation of squalene to gemcitabine as unique approach exploiting endogenous lipoproteins for drug delivery. Nat. Commun. 8, 15678.

Sobot, D., Mura, S., Rouquette, M., Vukosavljevic, B., Cayre, F., Buchy, E., Pieters, G., Garcia-Argote, S., Windbergs, M., Desmaele, D., et al., 2017b. Circulating Lipoproteins: A Trojan Horse Guiding Squalenoylated Drugs to LDL-Accumulating Cancer Cells. Mol. Ther. 25, 1596-1605.

Tabas, I., Williams Kevin, J., Borén, J., 2007. Subendothelial Lipoprotein Retention as the Initiating Process in Atherosclerosis. Circulation 116, 1832-1844.

Tadey, T., Purdy, W.C., 1995. Chromatographic techniques for the isolation and purification of lipoproteins. J. Chromatogr. B Biomed. Appl. 671, 237-253.

Thaxton, C.S., Rink, J.S., Naha, P.C., Cormode, D.P., 2016. Lipoproteins and lipoprotein mimetics for imaging and drug delivery. Adv. Drug Deliv. Rev. 106, 116-131.

Vitols, S., 1991. Uptake of low-density lipoprotein by malignant cells--possible therapeutic applications. Cancer Cells 3, 488-495.

Wasan, K.M., Cassidy, S.M., Ramaswamy, M., Kennedy, A., Strobel, F.W., Ng, S.P., Lee, T.Y., 1999. A comparison of step-gradient and sequential density ultracentrifugation and the use of lipoprotein deficient plasma controls in determining the plasma lipoprotein distribution of lipid-associated nystatin and cyclosporine. Pharm. Res. 16, 165-169.

Watanabe, J., Charles-Schoeman, C., Miao, Y., Elashoff, D., Lee, Y.Y., Katselis, G., Lee, T.D., Reddy, S.T., 2012. Proteomic profiling following immunoaffinity capture of high-density lipoprotein: Association of acute-phase proteins and complement factors with proinflammatory high-density lipoprotein in rheumatoid arthritis. Arthritis Rheum. 64, 1828-1837.

Yesylevskyy, S.O., Ramseyer, C., Savenko, M., Mura, S., Couvreur, P., 2018. Low-Density Lipoproteins and Human Serum Albumin as Carriers of Squalenoylated Drugs: Insights from Molecular Simulations. Mol. Pharm. 15, 585-591.

Zhang, Z., Chen, J., Ding, L., Jin, H., Lovell, J.F., Corbin, I.R., Cao, W., Lo, P.C., Yang, M., Tsao, M.S., et al., 2010. HDL-mimicking peptide-lipid nanoparticles with improved tumor targeting. Small 6, 430-437.

Zheng, G., Chen, J., Li, H., Glickson, J.D., 2005. Rerouting lipoprotein nanoparticles to selected alternate receptors for the targeted delivery of cancer diagnostic and therapeutic agents. Proc. Natl. Acad. Sci. U.S.A. 102, 17757.

Zhu, C., Xia, Y., 2017. Biomimetics: reconstitution of low-density lipoprotein for targeted drug delivery and related theranostic applications. Chem. Soc. Rev. 46, 7668-7682.